

XFEM Modelling and Experimental Observations of Foam Concrete Beam Externally-Bonded with KFRP Sheet

Malik Ridwan Maulana^a , Sugiman Sugiman^b , Hilton Ahmad^{a*} , Zainorizuan Mohd Jaini^a , Hazrina Mansor^c 

^a Department of Civil Engineering, Faculty of Civil Engineering and Built Environment, Universiti Tun Hussein Onn Malaysia, 86400 Parit Raja, Batu Pahat, Johor Darul Tak'zim, Malaysia. E-mail: hf200002@uthm.edu.my, hilton@uthm.edu.my, rizuan@uthm.edu.my

^b Faculty of Engineering, Department of Mechanical Engineering, University of Mataram, Mataram, Indonesia. E-mail: s.sugiman@unram.ac.id

^c School of Civil Engineering, Engineering Complex, Tunku Abdul Halim Muadzam Shah, Universiti Teknologi MARA, 40450 Shah Alam, Selangor Daru Ehsan, Malaysia. E-mail: hazrina4476@uitm.edu.my

* Corresponding author

<https://doi.org/10.1590/1679-78257205>

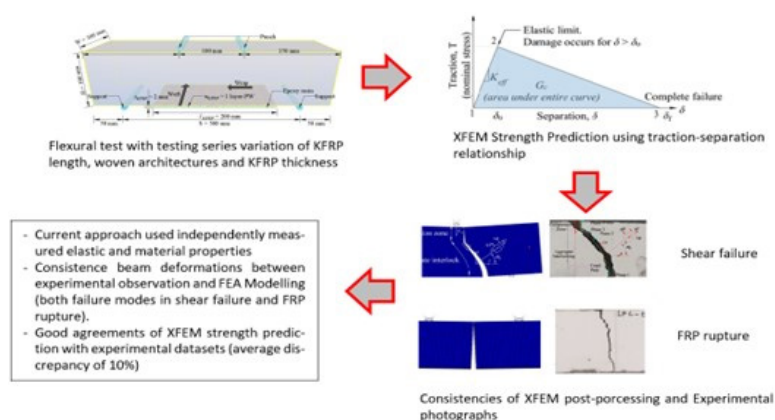
Abstract

This paper investigates the effect of KFRP composite sheets as a strengthening material in improving the load-carrying resistance of lightweight foam concrete beams using a FEA modelling framework. The study employed three parametric strengthening schemes (i.e., KFRP length, woven architecture types and KFRP thickness). Twenty-seven beam specimens were tested, and respective failure modes and ultimate load at failure were discussed. All the strengthened beam specimens failed mostly in shear mode and, to a lesser extent, in FRP rupture. Despite the absence of de-bonding failure, improvement of strengthening using KFRP sheet technique was exhibited. Later, Extended Finite Element Method (XFEM) Modelling was incorporated following failure mode exhibited. Strength predictions incorporating the traction-separation relationship using XFEM techniques. Validation work with experimental datasets showed good agreements with average discrepancies of less than 10%. The numerical approach can be used as a strength prediction tool in concrete beams with externally bonded FRPs.

Keywords

Foam concrete, Beam strengthening, FRP rupture, kenaf fiber composite, FEA Modelling.

Graphical Abstract



Received: July 29, 2022. In revised form: August 01, 2022. Accepted: August 29, 2022. Available online: August 30, 2022

<https://doi.org/10.1590/1679-78257205>



Latin American Journal of Solids and Structures. ISSN 1679-7825. Copyright © 2022. This is an Open Access article distributed under the terms of the [Creative Commons Attribution License](https://creativecommons.org/licenses/by/4.0/), which permits unrestricted use, distribution, and reproduction in any medium, provided the original work is properly cited.

1 INTRODUCTION

Concrete is a common housing and construction material due to its excellent mechanical strength, workability, formability, and integration of reinforcing bar as a structural element. Conversely, conventional concrete is heavy and prone to a dead load weight penalty. This drawback limits the use of concrete in high-rise buildings and poor foundation of bridge construction. Over the last decade, lightweight concrete such as foam concrete has gained popularity in the construction sector due to its low density and comparable specific strength to conventional concrete. Despite its growing popularity, foam concrete has few drawbacks, including low mechanical properties, inferior durability, and excessive drying shrinkage due to its porous microstructures (She et al., 2018). Hashim & Tantray (2021) investigated the foaming agent types, and the result showed that the protein-based foam performed better than the synthetic foam counterparts. Similar agreements were reported by Sun et al. (2018), which showed that the synthetic-based foam has better shear strength than the plant and animal surfactants. Correlation between the compressive strength and density of the foam concrete has been reported by (Lee et al. (2018), Gökçe et al. (2019), Ahmad et al. (2019), Nambiar & Ramamurthy (2006), Hilal et al., (2016), Bagheri & Samea, (2019), Liu et al., (2014) and depicted in Figure 1(a). Meanwhile, Figure 1 (b) shows the effects of porosity to the compressive strength of foam concrete, as reported by Oren et al. (2020), Sang et al. (2015), She et al. (2018), Liu et al., (2014).

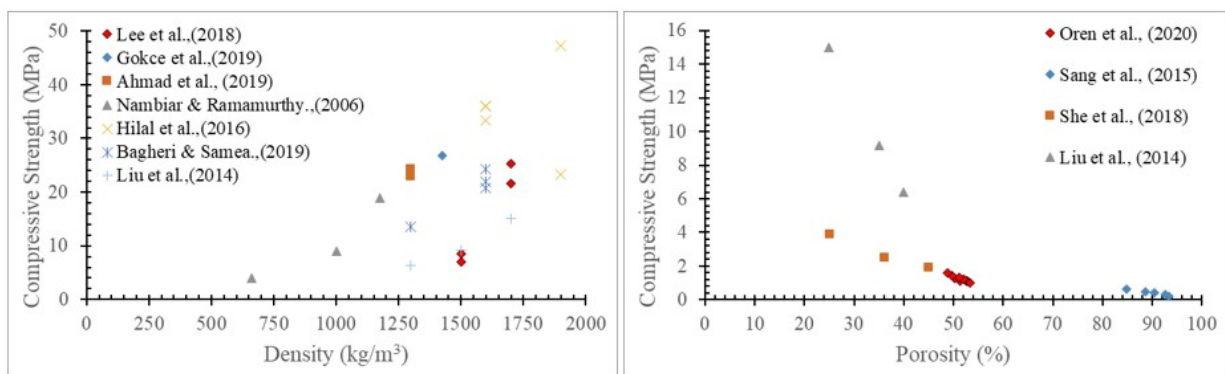


Figure 1 Mechanical properties of Foam concrete (a) Compressive Strength-density (b) Compressive Strength-porosity.

Flaws in foam concrete are commonly generated by voids formed during the casting process, mixing bubble foam and water, and shrinkage cracking. Those flaws cause high stress at the crack tip during the fracture process. Nevertheless, a strengthening strategy in foam concrete beams under flexural load is required to enhance the beam resistance. Various guidelines such as in (440.2R-02, (2002), Lecture & Czaderski, (2013), FIB, (2001), Japan Society of Civil Engineers (JSCE), (2001) provides closed-form expressions on transition from shear failures to cohesive de-bonding modes on conventional concrete with CFRP strengthening. A study by Huang et al. (2015) on notched beams strengthened with CFRP found that CFRP sheet length contributes to ultimate load capacity and the associated failure modes (i.e, shear and debonding failure modes). Additionally, the investigation by Junaid et al. (2020) on reinforced concrete beams strengthened with CFRP sheets claimed that the longer strengthening demonstrated the CFRP rupture; however, the shorter strengthening indicated the debonding failures between CFRP and concrete beam. In addition, Al-Rousan et al. (2018) investigated beam strengthening with CFRP with and without anchorage. It was found that the anchorage system played a significant effect in decreasing the crack width and crack length to demonstrates delay upon debonding within the CFRP sheet.

The utilization of natural fibre to replace synthetic fibres has been gaining great attention. Many studies have found that natural fibres offered promising results in replacing synthetic fibres (Misonon et al., 2014). A kenaf fibre treated using various chemical treatments could enhance its mechanical properties (Mahjoub, Yatim, Mohd Sam, & Hashemi, 2014a). Further, Mahjoub, Yatim, Mohd Sam, & Raftari (2014b) reported that increasing the fibre volume fraction resulted in an increase in tensile modulus and a reduction in the ultimate tensile strain. The optimum fibre weight fraction to obtain the maximum tensile load at failure was 40%. Abdul et al. (2014) investigated different polymer matrix types in kenaf fibre reinforced polymer composites to strengthen the reinforced beams and found that epoxy polymer performed better in load-carrying capacity compared to polyester and vinyl ester.

Finite Element (FE) is an alternate method for characterising the damage behaviour of engineering structures. The damage behaviour of a material can be represented by using the traction-separation law (TSL) as constitutive model. Various modelling techniques can be incorporated with TSL, such as the extended finite element method (XFEM), virtual crack closure technique (VCCT) and cohesive zone model (CZM). A study by H. Ahmad et al., (2021) investigate the three-point

bending foam concrete beam using XFEM and CZM method and found that XFEM performed better than the CZM in predicting the load capacity. While Yu et al., (2021) simulating beam nuclear graphite by using the XFEM, the CZM and the VCCT methods. Their findings showed that, compared to the XFEM and the CZM, the VCCT is more sensitive to mesh size.

Few factors are considered when improving the capability of natural fibre composites for reinforcing foam concrete, including the strengthening length, woven architectures types, and FRP thickness. However, comprehensive studies of those factors are rarely reported. As expected, application of FRP sheet bonded entirely within beam tension face is costly and ineffective. This study aims to conduct experimental work and investigates the behaviour of strengthened concrete beams with KFRP sheets, later strength predictions were performed by adopting TSL relationship and XFEM technique.

2 FABRICATION OF FOAM CONCRETE BEAM

2.1 Mix Design of Foam Concrete

The lightweight foam concrete was batched according to a specific gravity mix design. The lightweight foam concrete was composed of river sand with a maximum diameter of 3 mm, Portland cement CEM I-42.5R, silica fume (SF) as partial cement replacement, superplasticizer (SP) and clean tap water. Silica fume was manufactured by Shinjiang Shengping Minerals Co., Ltd. The Sika Aer 50/50 is a synthetic-based foam agent mixed with a ratio of a foaming agent to water as 1:20. A foam generator was used to generate the pre-foam. Superplasticizers were used to compensate for the water requirements for sufficient workability. Table 1 showed the mix proportion for 1 m³ of foam concrete where water: binder, binder: sand, SP: binder ratios were 0.42, 3, 0.01, respectively, while the SF content was 5 wt%. Prior to the foam addition, a base mix density of 2010 kg/m³ was measured, and a density of 1820 kg/m³ was targeted with the addition of foam. Upon reaching target density, the concrete is poured into steel beam moulds and allowed to be set at least 24 hours. Upon the mould stripping, all specimens were placed in water curing tank for 28 days. Fabrication of foam concrete beam is shown in Figure 2.

Table 1 Mix-design of foam concrete.

Binder (kg/m ³)		Sand (kg/m ³)	Superplasticizers (kg/m ³)	Water (kg/m ³)	Foam (liter/m ³)	f_c (MPa)
Cement	SF					
1043.91	54.94	366.28	10.99	461.52	105	39.6



(a)



(b)



(c)

Figure 2: Fabrication of foam concrete beam (a) foam generation (b) casting of foam concrete (c) water-cured for 28-days.

2.2 Production of KFRP Sheet and Mechanical Testing

Kenaf yarns were weaved using a handloom machine with good precisions and care to form a weaving pattern of plain-woven fabric kenaf (276 tex). The packing density in warp and weft directions for plain weave (PW), twill weave (TW), and five harness satin (FHS) are shown in Figure 3. The aerial size of each woven fabric sheet weaving layer was approximately 250 x 250 mm². Epoxy resin was used as a matrix binder, commercially known as Sikadur-31 SBA S02, which was based on Bisphenol-A with a hardener of trimethylhexane. The epoxy took at least 24 hours to cure at room temperature. Current experimental work used epoxy resin to hardener ratio of 3:1.

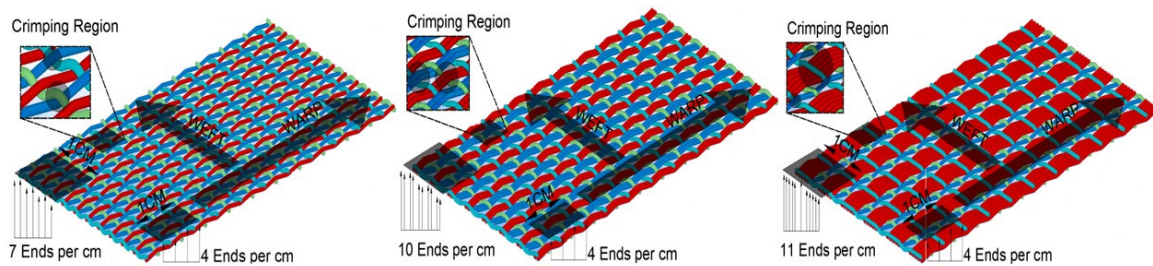


Figure 3: Architecture of kenaf fiber yarn (a) Plain weave (PW), (b) Twill (TW) and (c) Five harness satin (FHS).

Figure 4 depicts the phases involved in installing the KFRP sheet on the tension concrete beam surface prior to four-point bending test (4PBT) on the 28th day of concrete age. The process involved marking and surface roughing before placing KFRP onto the beam surface to ensure adequate bonding between the concrete and adhesive layer. Then, the beam specimen was white-painted for better visibility for cracking formation. 2 mm thick aluminium edging was used as a railing within the KFRP sheet to control the KFRP thickness upon matrix setting. The epoxy adhesive was smeared uniformly in each KFRP layer and allowed to be set for at least three hours. A quasi-static four-point bending test was performed on a foam concrete beam using a 100 kN load-cell capacity Instron UTM machine with a crosshead speed of 0.5 mm/min following ASTM-D6272 (2008). The ultimate loads and failure modes for each testing series were recorded, and three testing specimens from each series were averaged accordingly.

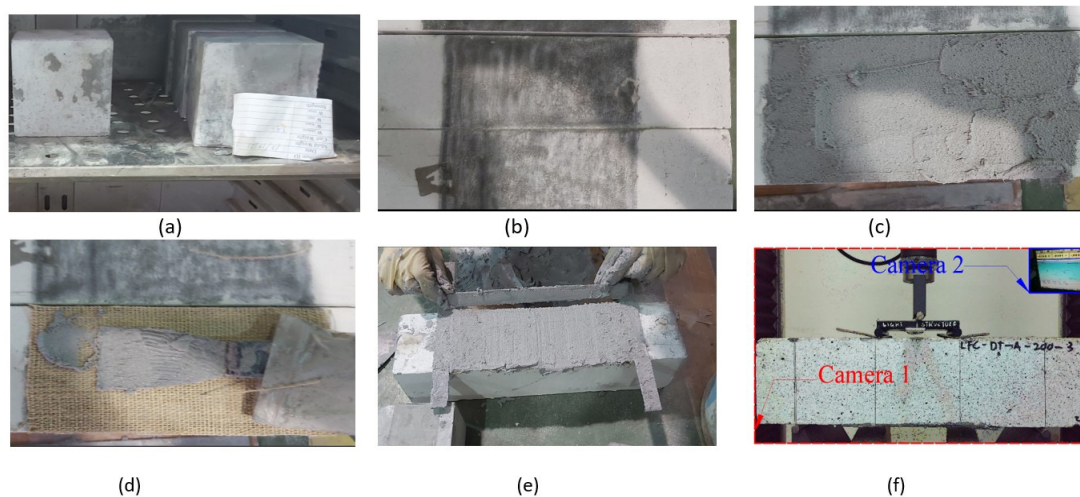


Figure 4: KFRP placing and experimental testing of foam concrete beam strengthened with KFRP sheet (a) Oven-dry for 24 hours, (b) Painting & Surface treatment, (c) smeared 1st layer Epoxy (d) laying KFRP & smeared 2nd layer Epoxy (e) KFRP placing sheet (f) 4PBT test under quasi-static load.

2.3 Testing Series Investigated

The lightweight foam concrete (LFC) specimens with a density of 1750 kg/m^3 strengthened with the KFRP sheet were produced and tested. Three specimens in each testing series were prepared for the four-points bending test. The testing series included various KFRP sheet lengths (Series A), woven fabric architectures (Series B) and KFRP sheet thickness (Series C). The Series A consisted of 100, 150, 200 and 250 mm long with a fixed width of 100 mm of plain weave architectures. Subsequently, Series B comprised of different woven architectures types, i.e., plain weave (PW), twill weave (TW) and five harness satin (FHS) with a constant KFRP length of 200 mm. Finally, the Series C has different KFRP thickness of one layer (PW1), two layers (PW2) and four layers (PW4). Note that a similar concrete designation was used for 200 mm length (series A), plain weave (Series B) and one layer KFRP (PW1) and therefore, identical experimental datasets were used for results evaluation. All series were cast in a single batching to allow mixture consistency for a reliable comparison. Figure 5 depicts the basic geometries of strengthened beam specimens, and different variables tested with beam designations are given in Table 2. Apparent porosity was measured by the dry-wet weight of the beam specimen. Note that a width 100 mm woven fabric composite plate was adhesively bonded at the tension face of foam concrete beam with a dimension of $400 \times 100 \times 100 \text{ mm}^3$.

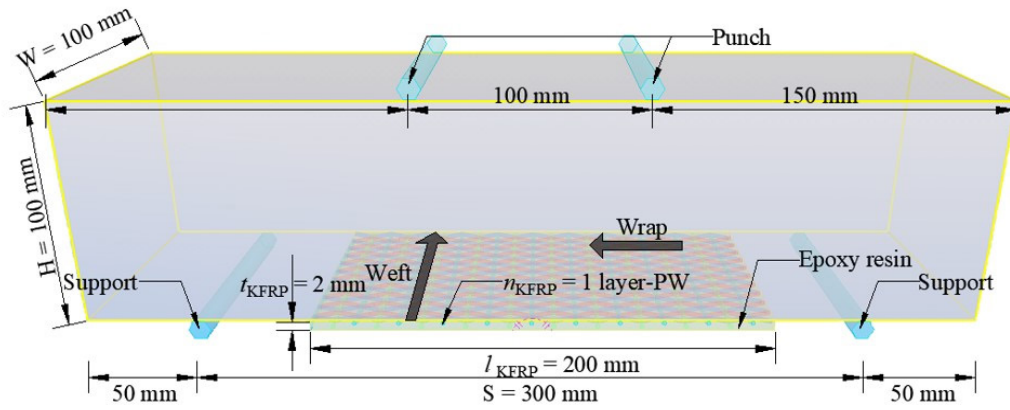


Figure 5: Geometry on foam concrete beam strengthened with KFRP.

Table 2 Detail of each series model.

Designation	KFRP Length (mm)	KFRP Thickness (mm)	KFRP Layer	Test method	Porosity (%)
Control	-	-	-	4PBT	17 ± 0.764
A-100	100	2	1 layer-PW	4PBT	20 ± 2.255
A-150	150	2	1 layer-PW	4PBT	20 ± 1.155
A-200/B-PW/C-PW1	200	2	1 layer-PW	4PBT	21 ± 1.521
A-250	250	2	1 layer-PW	4PBT	16 ± 1.893
B-TW	200	2	1 layer-TW	4PBT	16 ± 1.127
B-FHS	200	2	1 layer-FHS	4PBT	19 ± 3.132
C-PW2	200	3	2 layer-PW	4PBT	17 ± 0.382
C-PW4	200	5	4 layer-PW	4PBT	19 ± 1.665

3 RESULTS

3.1 Crack and Failure Modes

Figure 6 depicts the failure mechanism and fracture patterns that occurred during mechanical testing. The flexural fracture in all beams is initiated from the bottom surface of the beam mid-span (within the constant moment zone) for FRP rupture. In contrast, under shear failure, the crack is initiated from the KFRP sheet edge and then diagonally propagated toward the point of the applied load. It can be seen that the failure modes were determined by KFRP sheet adhesively-bonded to concrete beam either by intrinsic factors such as KFRP sheet geometries and/or material properties.



(a) Flexural failure Control concrete



(b) Shear Failure from C-PW2



(c) FRP fracture from specimen A-250

Figure 6: Photographs of the fracture specimens (a) control concrete (b) shear failure (c) FRP rupture

3.2 Ultimate Load Various Series

The ultimate load and ultimate deflection of all testing series investigated are given in Figure 7 and Figure 8, respectively. With regards to Series A (various KFRP sheet lengths), the ultimate load increased as longer KFRP sheets were used. The enhancement in the ultimate load was 5%, 42%, 102% and 154% for the beam with KFRP lengths of 100 mm, 150 mm, 200 mm and 250 mm, respectively. In Series A, the FRP rupture mode was seen with concrete strengthened with 250 mm KFRP sheet length, but the remaining KFRP sheet lengths failed in shear failures (i.e., 100 mm, 150 mm and 200 mm). This phenomenon has similar findings with study conducted by Ding et al., (2014) where CFRP lengths of less than 200 mm exhibited shear failure. Respective to Series B (various woven fabric architectures), all beam specimens failed in shear modes, but the ultimate load differs significantly. This phenomenon occurred due to the woven fabric arrangement in the KFRP sheet, and the applied loading is resisted by reinforcing fibres arranged in the warp direction. It is worth noting that all woven KFRP types has different numbers of warp yarns but has constant orthogonally weft yarns. Compared to the control specimen, the enhancement is 78% and 126% for the TW and the FHS, respectively. All testing specimens in Series C with different KFRP sheet thicknesses demonstrated shear failure, but to less extent, the ultimate load was affected by KFRP sheet thickness. As seen in Figure 8 (c), the ultimate displacement was highest in thinner sheets, allowing the concrete beam to bend more under applied load.

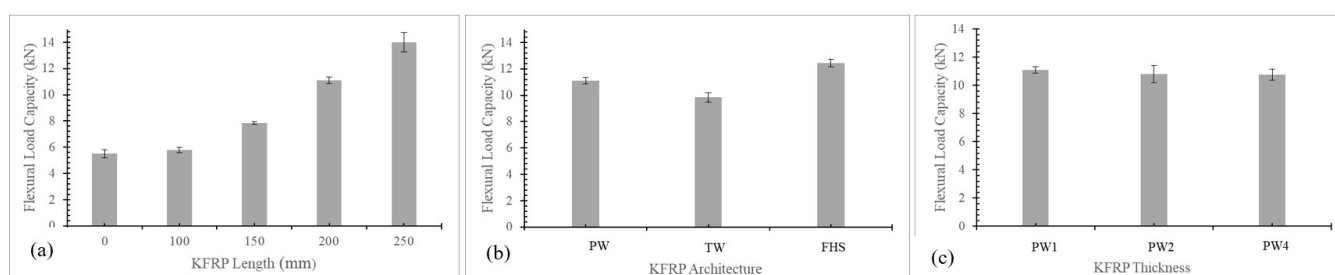


Figure 7: The ultimate flexural load in (a) Series A (b) Series B (c) Series C.

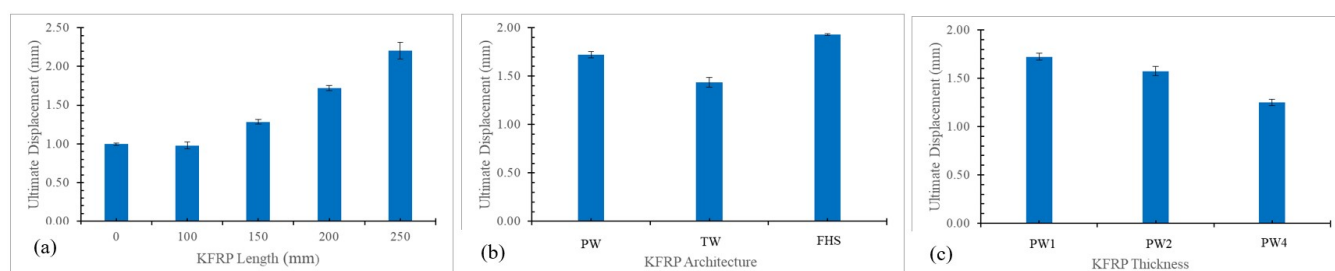


Figure 8: The ultimate displacement of each series (a) Series A (b) Series B (c) Series C.

3.3 Performance Evaluation

The testing concrete series were evaluated in terms of elastic stiffness (k_E), energy absorption (EA), strength factor (SF) and displacement factor (DF) and performance factor (PF), which are tabulated in Table 3. Elastic stiffness is defined as the slope in load-displacement curve extracted from data-logger prior to crack initiation. Regarding to Series A, the elastic stiffness increased with longer KFRP sheet. Compared to the control beam, the stiffness enhancement was 17%, 24%, 32% and 41% for lengths of 100 mm, 150 mm, 200 mm and 250 mm, respectively. Meanwhile, in Series B, stiffness enhancement was 32%, 36% and 27% in the PW, the TW and the FHS architectures, respectively. This condition is due to respective material properties, especially to elastic modulus (E), as they have different fiber volume fraction associated to yarns arrangement. Lastly, in Series C, the enhancement of stiffness due to KFRP thicknesses was 34% and 36% for PW2 and PW4, respectively, compared to the un-strengthened beam.

Energy absorption was estimated as the area under the load-displacement curve. In Series A, the effect of KFRP length on the energy absorption showed significant increments of 19%, 89%, 286% and 521% in KFRP length of 100 mm, 150 mm, 200 mm and 250 mm, respectively. While in Series B, the enhancement of energy absorption was 286%, 187% and 387% for the PW, the TW and the FHS, respectively. It can be seen that FHS has the most superior energy absorption compared to other woven fabric types. Although energy adsorption is associated with more significant number of crimping regions, but the larger volume of yarns fibres in the warp direction leads to higher energy absorption. In Series C, the energy absorption enhancement was 243% and 246% for PW2 and PW4, respectively. It seems that the effect of

sheet thickness is insignificant. This is because the fiber volume fraction is not significant respective to sheet thickness (note that the fiber arrangements are similar to each plain weave fiber stacked).

The performance of structural elements is represented by evaluating the strength (load capacity) and deformability (displacement). The strength and the deformability of the strengthened concrete beam was computed by calculating the strength factor (*SF*) and deformability factor (*DF*). The *SF* and the *DF* in this study were calculated by obtaining normalized ultimate load (and displacement respectively) of strengthened concrete beam to un-strengthened beam (control). The performance factor (*PF*) evaluates the overall structural performance by multiplying the strength factor (*SF*) and deformability factor (*DF*). In Series A, the enhancement in terms of *PF* was 3%, 83%, 248% and 462 (equivalent to *PF* of 1.033, 1.833, 3.484 and 5.617) for lengths of 100 mm, 150 mm, 200 mm and 250 mm, respectively. Regarding Series B, the enhancement of *PF* was 248%, 157% and 336% (equivalent *PF* of 3.484, 2.569 and 4.363) for PW, TW and FHS, respectively. Meanwhile, in Series C, the enhancement of *PF* was 210% and 145% for PW2 and PW4, respectively.

Table 3. Parameters output and performance evaluation.

Specimen ID	Elastic Stiffness (k_E), kN/mm	Energy Absorption (EA), kNmm	Strength Factor (SF)	Displacement Factor (DF)	Performance Factor (PF)
Control	8.377 ± 0.894	1.683 ± 0.427	1 ± 0	1 ± 0	1 ± 0
A-100	9.762 ± 1.838	2.006 ± 0.305	1.051 ± 0.034	0.983 ± 0.044	1.033 ± 0.047
A-150	10.420 ± 0.239	3.183 ± 0.114	1.422 ± 0.022	1.289 ± 0.031	1.833 ± 0.071
A-200/B-PW/C-PW1	11.048 ± 0.193	6.479 ± 0.612	2.016 ± 0.043	1.728 ± 0.035	3.484 ± 0.118
A-250	11.813 ± 1.676	10.441 ± 1.641	2.543 ± 0.134	2.209 ± 0.108	5.617 ± 0.415
B-TW	11.421 ± 0.793	4.833 ± 0.652	1.784 ± 0.068	1.438 ± 0.050	2.569 ± 0.186
B-FHS	10.640 ± 0.644	8.190 ± 0.640	2.257 ± 0.055	1.934 ± 0.010	4.363 ± 0.125
C-PW2	11.200 ± 0.593	5.744 ± 0.820	1.962 ± 0.108	1.962 ± 0.108	3.098 ± 0.252
C-PW4	11.352 ± 1.689	5.816 ± 0.739	1.953 ± 0.069	1.953 ± 0.069	2.449 ± 0.121

Although none of the strengthened beam specimens failed in cohesive failures within the adhesive layer, the porous nature of foam concrete beam is prone to brittle shear failure and FRP fracture. Nevertheless, this study can be used as an early feasibility study of KFRP sheets as strengthening material in foam concrete. Future research should explore the applicability of these materials to a greater extend.

4 FINITE ELEMENT MODELLING WORKS

Strength prediction works under four-point bending tests were performed using finite element software ABAQUS CAE 2021 following the testing series above. Five components were assembled to conform testing set-up under four-points bending test comprised of a concrete beam with four analytical rigid wire punches and supports. As described in the testing series above, the KFRP sheet has a similar width to a foam concrete beam. A total of nine 2-D models were developed. The cracked beam body was assigned with reduced four-node plain-strain elements (ABAQUS designation as CPE4R), and coupling from both rigid analytical punch was assigned to a control set to allow uniform controlled displacement. A pin and roller supports were assigned with respective degrees of freedom to represent a simply supported beam tested under quasi-static loading. Extended Finite Element Method (XFEM) technique using Maximum principal stress criterion (MaxPS) was implemented.

4.1 Elastic and Material Properties

Incorporation of the traction-separation relationship as a constitutive model requires independent elastic and material properties input during pre-processing stage (i.e., un-notched strength (σ_0), elastic modulus (E), Poisson's ratio (ν), and fracture energy (G_F)). The foam concrete properties is a concrete subset investigated from Maulana et al., (2022) and KFRP sheet properties are subset from Omar et al. (2022), both are tabulated in Table 4 and 5 respectively. These properties were independently measured from an independent experimental setup following a code of practices. Three specimens were tested with good consistencies, and respective standard deviations are also given accordingly.

Table 4. Material properties of foam concrete with density 1700 kg.m^3 (after Maulana et al., (2022)).

Elastic Properties		Material Properties	
Elastic Modulus, E (MPa)	Poisson's Ratio, ν	Un-notched flexural beam strength, σ_0 (MPa)	Fracture Energy, G_F (N/mm)
13000	0.28	1.652	0.015

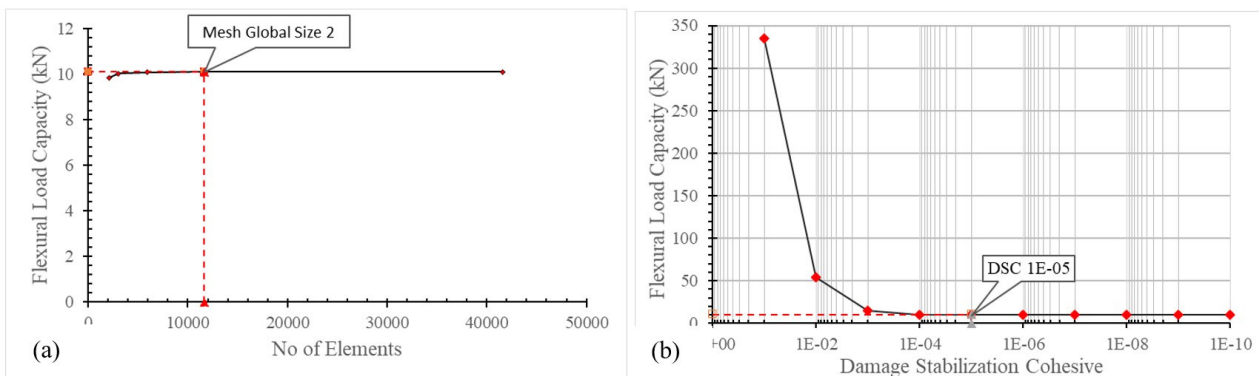
Table 5. Material properties of KFRP sheet (after Omar et al., (2022)).

Lay-up Designations	Elastic Properties		Material Properties	
	Elastic Modulus, E (MPa)	Poisson's Ratio, ν	Un-notched strength, σ_0 (MPa)	Fracture Energy, G_F (N/mm)
PW	6212 ± 189	0.214 ± 0.005	24.96 ± 0.4	6.301 ± 1844
TW	6034 ± 134	0.225 ± 0.004	28.80 ± 0.6	7.646 ± 2048
FHS	5876 ± 107	0.237 ± 0.005	30.65 ± 0.8	10.691 ± 2827
PW2	4637 ± 67	0.254 ± 0.007	31.84 ± 1.3	11.309 ± 2673
PW4	2871 ± 174	0.277 ± 0.005	38.18 ± 2.2	21.507 ± 2545

4.2 Sensitivity Study

The strength prediction works should be independent of mesh size and damage stabilization coefficient effects. First sensitivity study refining the meshing region at the vicinity area of the cracked beam as a regional area of interest. This sensitivity study used concrete designation model A-250 series. From basic FEA fundamentals, a large mesh size is associated with high computational effort but usually produces less accurate results. On the contrary, finer mesh promotes excellent accurate result but requires large computational times and resources. In the respective to mesh sensitivity, global mesh sizes ranging between one to five were investigated (smaller mesh density corresponds to a higher number of elements). It was found that strength prediction is insensitive to the mesh refinements as the current modelling approach was driven by an energetic approach, as shown in Figure 9 (a).

A second sensitivity study was damage stabilization coefficients; a large coefficient is associated with easy convergence but gives ill-physical behavior leading to outrageous predictions. On the contrary, a small damage stabilization coefficient leads to convergence difficulties, therefore, a reasonable damage tolerances coefficient is required. Figure 9 (b) showed that strength predictions began to show plateau flexural load at failure at damage stabilization coefficient of 1×10^{-5} (here, a consistence global mesh size of two was used). Consistency use of mesh size and damage stabilization coefficients were used in all other models.

**Figure 9:** A sensitivity study on (a) Mesh refinement, (b) Damage stabilization coefficient.

4.3 Damage Plot under Shear Failure

The concrete designation A-200 was chosen to represent a typical post-processing output in shear mode failure. Respective load-displacement profile was plotted in Figure 10 with damage plot at labelled key-points are subsequently given in Figure 11. Under shear failure, a crack was initiated at the KFRP sheet edge tip due to large peel stress exhibited. In general, as peel stress reached maximum principle tensile strength of foam concrete, the crack initiates and propagates to under point load. Due to further distances from the KFRP edge to punch, diagonal crack is exhibited. Here, the effect from root fillets at both KFRP edges is ignored.

At Point A, it is predicted that micro-damages events take place in the form of matrix cracking, aggregate interlocking and crack bridging, and crack initiating at a certain distance prior to ultimate load at the failure to give catastrophic failure. Ultimate load at failure is given at Point B, approximately at two-thirds of beam depth and here recorded as strength prediction. At Point C, catastrophic failures occurred and followed by beam separation at point D. It was found that the shear failure confirmed the shear mechanism described in (NCHRP-549, 2005). According to the guidelines, the bottom diagonal crack path is highly associated with aggregate interlocking to give ultimate load at failure. Meanwhile, the top crack path is known as shear in the compression zone, where both crack paths are shown in Figure 11(d). Note that the current XFEM modelling approach assumes homogeneous properties, which may lead to improper exhibition of beam deflection as seen experimentally. Additionally, the KFRP sheet is regarded as perfectly symmetrical configuration during set-up prior to mechanical testing (it always showed some eccentricity during mechanical testing).

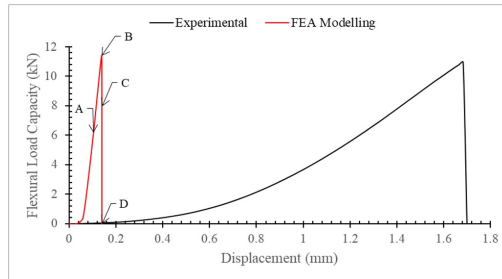


Figure 10: Typical load-displacement profile with shear failure mode (here given in concrete designation A-200).

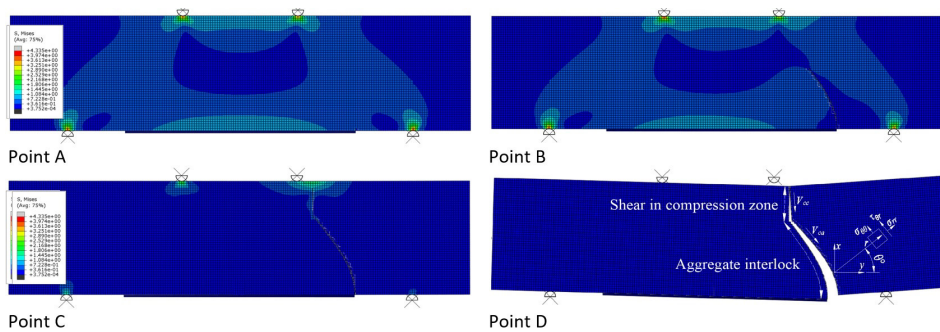


Figure 11: Damage plot under shear failure mode at key points labelled in Figure 10.

4.4 Damage Plot under FRP Rupture

Figure 12 shows the load-displacement curve and later plotted with damage illustration extracted from post-processing output from XFEM Modelling with FRP fracture mode in Figure 13. Only one concrete designation that failed in FRP fracture, i.e., A-250. Prior to Point A, a linear elastic curve is exhibited, and the crack has not been initiated. Due to composite action between foam concrete beam and KFRP plates, both showed similar deformation (i.e., equal strain, $\epsilon_c = \epsilon_{KFRP}$ is exhibited). Subsequently, the concrete beam started to initiate damage at the mid-span (as given in Point A) until reaching a certain length and due to the strengthening from KFRP to transfer the applied stress to concrete through friction. Now the applied stress is borne by the adjacent KFRP sheet as shown in region B-C. Subsequently, as fracture energy of KFRP sheet exceeds, the fracture and failure in KFRP sheet as seen in Point C to give ultimate load at failure corresponding to catastrophic failure. Finally, beam separation at the mid-span occurred at Point D.

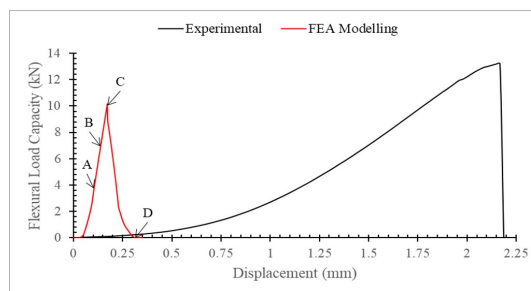


Figure 12: Typical load-displacement profile with FRP fracture failure mode (as given in A-250).

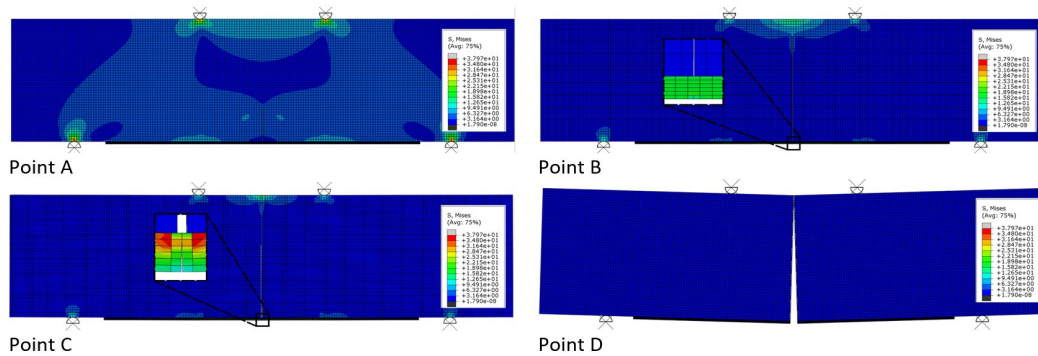


Figure 13: Damage plot under FRP flexural failure mode at the key points labelled in Figure 12.

4.5 Validation of XFEM Modelling with Experimental Datasets

This section validates the strength prediction (i.e., ultimate load at failure) from XFEM modelling with experimental datasets. Table 6 shows the discrepancies between experimental datasets and FEA Modelling. Noted that an average of 10% discrepancy were shown and regarded as good agreement. From Table 6, Series A (i.e., KFRP length ranging from 100 to 200 mm) showed smaller discrepancies as the KFRP sheet gets longer in shear failure mode. The KFRP length is prone to exhibit larger bending in longer KFRP sheets to promote favorable strengthening effect. The current approach assumed KFRP as homogeneous material, which is more represented in longer KFRP behavior as better KFRP deformation exhibited.

On the other hand, concrete beam A-250 exhibited FRP rupture and showed under-predicted strength from XFEM modelling. It has been assured that the beam deformation is consistency with experimental observations of FRP fracture. The fracture energy values of KFRP and foam concrete are independently measured as a subset of materials reported in Omar et al. (2022).

Series B showed discrepancies ranging from 2 to 14%; the variances between these series are woven architecture types to include plain weave, twill weave, and five harness satin. Similar modelling techniques and approaches were used, with the sole variation being the integration of measured elastic and material properties from independent experimental work (again, KFRP sheet and foam concrete are a subset of previously reported literatures in (Maulana et al., (2022) and Omar et al., (2022)). Although inconsistent nature of natural fibres may exhibit, less than 15% of discrepancies were recorded in this series.

Series C revealed good agreements (with discrepancies between 2 - 3%) were seen as KFRP thickness was varied. The KFRP sheet thickness is modelled as the nominal thickness and independently measured elastic and material properties as given in Table 5. It is expected that better prediction is exhibited in thicker plates. However, due to the exhibition of shear failure modes in all tested specimens, the effect of KFRP bending is not much appreciated due to insignificant contribution from KFRP deformation to ultimate load at failure.

Table 6. Discrepancy between Experimental Observation and FEA Modelling.

Specimen ID	P Experimental (kN)	P FEA Modelling (kN)	Discrepancy (%)
A-100	5.789 ± 0.186	6.944	19.958
A-150	7.832 ± 0.120	8.336	6.443
A-200*	11.102 ± 0.236	11.389	2.581
A-250	14.002 ± 0.738	10.153	-27.485
B-PW*	11.102 ± 0.236	11.389	2.581
B-TW	9.826 ± 0.372	11.245	14.451
B-FHS	12.427 ± 0.303	12.930	4.051
C-PW1*	11.102 ± 0.236	11.389	2.581
C-PW2	10.804 ± 0.594	11.170	3.393
C-PW4	10.755 ± 0.382	11.166	3.823

* these concrete designations are taken from similar specimens as all series were batched in a single mixture.

5 CONCLUSIONS

The effect of KFRP lengths on the ultimate load capacity is significant. Only specimens with a KFRP length of 250 mm demonstrated FRP fracture, and the remaining KFRP sheet length exhibited shear failure mode. The concrete beams strengthened with various woven fabric architectures showed that all beam specimens failed under shear, but woven fabric architectures with high fiber volume fraction demonstrated higher ultimate load. Here, FHS showed excellent ultimate load at failure and ultimate displacement compared to other architecture types. The concrete beam strengthened with the KFRP sheet thickness showed that the thinner sheets promote excellent ultimate load at failure as the concrete beam could deform significantly before failure. Later, strength predictions were performed within XFEM modelling incorporating the traction-separation relationship. This work independently measured elastic and material properties as a material subset from published literature. There were good agreements between FEA modelling and experiment datasets with average discrepancies of 10%.

6 ACKNOWLEDGEMENT

This research was financially supported by Ministry of Higher Education Malaysia (MOHE) through Fundamental Research Grant Scheme (FRGS/1/2020/TK01/UTHM/02/4). We also want to thank to Research Management Centre (RMC), University Tun Hussein Oon Malaysia (UTHM) for sponsoring this work under Postgraduate Research Grant (GPPS) (Research Grant No.H706).

Author's Contributions: Conceptualization, M.R. Maulana, H Ahmad, S Sugiman, ZM Zaini, H Mansor Methodology, H Ahmad, S Sugiman; ZM Jaini Investigation, M.R. Maulana, H Ahmad, S Sugiman Writing - original draft, M.R. Maulana, H Ahmad; Writing – Review and Editing, S Sugiman, H Mansor Funding Acquisition, H Ahmad; Supervision, H Ahmad.

Editor: Marco L. Bittencourt

References

- 440.2R-02, A. (2002). Guide for the Design and Construction of Externally Bonded FRP Systems for Strengthening Concrete Structures Reported by ACI Committee 440. *Acj*, 440, 45.
- Abdul, N. H. K., Bhutta, M. A. R., Jamaludin, M. Y., Warid, M. H., Ismail, M., Rahman, M. S., Yunus, I., & Azman, M. (2014). Kenaf fiber reinforced polymer composites for strengthening RC beams. *Journal of Advanced Concrete Technology*, 12(6), 167–177. <https://doi.org/10.3151/jact.12.167>
- Ahmad, H., Sugiman, S., Jaini, Z. M., & Omar, A. Z. (2021). *Numerical Modelling of Foamed Concrete Beam under Flexural Using Traction-Separation Relationship*. 18(5), 1–13.
- Ahmad, M. R., Chen, B., & Farasat Ali Shah, S. (2019). Investigate the influence of expanded clay aggregate and silica fume on the properties of lightweight concrete. *Construction and Building Materials*, 220, 253–266. <https://doi.org/10.1016/j.conbuildmat.2019.05.171>
- Al-Rousan, R. Z., Alhassan, M. A., & AlShuqari, E. A. (2018). Behavior of plain concrete beams with DSSF strengthened in flexure with anchored CFRP sheets—Effects of DSSF content on the bonding length of CFRP sheets. *Case Studies in Construction Materials*, 9, e00195. <https://doi.org/10.1016/j.cscm.2018.e00195>
- ASTM-D6272. (2008). *Standard Test Method for Flexural Properties of Unreinforced and Reinforced Plastics and Electrical Insulating Materials by Four-Point Bending 1*. 1–9. <https://doi.org/10.1520/D6272-10.1>
- Bagheri, A., & Samea, S. A. (2019). Role of non-reactive powder in strength enhancement of foamed concrete. *Construction and Building Materials*, 203, 134–145. <https://doi.org/10.1016/j.conbuildmat.2019.01.052>
- Ding, J., Wang, F., Huang, X., & Chen, S. (2014). *The Effect of CFRP Length on the Failure Mode of Strengthened Concrete Beams*. 1705–1726. <https://doi.org/10.3390/polym6061705>
- FIB. (2001). Externally bonded FRP reinforcement for RC structures. In *International Federation for Structural Concrete (fib)* (Vol. 14). <http://scholar.google.com/scholar?hl=en&btnG=Search&q=intitle:Externally+bonded+FRP+reinforcement+for+RC+structures#0>
- Gökçe, H. S., Hatungimana, D., & Ramyar, K. (2019). Effect of fly ash and silica fume on hardened properties of foam concrete. *Construction and Building Materials*, 194(112), 1–11. <https://doi.org/10.1016/j.conbuildmat.2018.11.036>

- Hashim, M., & Tantray, M. (2021). Comparative study on the performance of protein and synthetic-based foaming agents used in foamed concrete. *Case Studies in Construction Materials*, 14, e00524. <https://doi.org/10.1016/j.cscm.2021.e00524>
- Hilal, A. A., Thorn, N. H., & Dawson, A. R. (2016). Failure mechanism of foamed concrete made with/without additives and lightweight aggregate. *Journal of Advanced Concrete Technology*, 14(9), 511–520. <https://doi.org/10.3151/jact.14.511>
- Huang, X., Wang, J., Zhang, F., Niu, S. S., & Ding, J. (2015). An Experimental Investigation on the Failure Behavior of a Notched Concrete Beam Strengthened with Carbon Fiber-Reinforced Polymer. *International Journal of Polymer Science*, 2015. <https://doi.org/10.1155/2015/729320>
- Japan Society of Civil Engineers (JSCE). (2001). *Recommendations for upgrading of concrete structures with use of continuous fiber sheets*. 88.
- Junaid, M. T., Elbana, A., & Altoubat, S. (2020). Flexural response of geopolymer and fiber reinforced geopolymer concrete beams reinforced with GFRP bars and strengthened using CFRP sheets. *Structures*, 24(January), 666–677. <https://doi.org/10.1016/j.istruc.2020.02.003>
- Lecture, E. T. H., & Czaderski, C. (2013). *Flexural strengthening of reinforced concrete Swiss Code 166 and other codes / guidelines Literature : Codes / Guidelines*. November, 1–104.
- Lee, Y. L., Tan, C. S., Lim, S. K., Mohammad, S., & Lim, J. H. (2018). Strength Performance on Different Mix of Cement-Sand Ratio and Sand Condition for Lightweight Foamed Concrete. *E3S Web of Conferences*, 65, 1–10. <https://doi.org/10.1051/e3sconf/20186502006>
- Liu, M. Y. J., Alengaram, U. J., Jumaat, M. Z., & Mo, K. H. (2014). Evaluation of thermal conductivity, mechanical and transport properties of lightweight aggregate foamed geopolymer concrete. *Energy and Buildings*, 72, 238–245. <https://doi.org/10.1016/j.enbuild.2013.12.029>
- Mahjoub, R., Yatim, J. M., Mohd Sam, A. R., & Hashemi, S. H. (2014a). Tensile properties of kenaf fiber due to various conditions of chemical fiber surface modifications. *Construction and Building Materials*, 55, 103–113. <https://doi.org/10.1016/j.conbuildmat.2014.01.036>
- Mahjoub, R., Yatim, J. M., Mohd Sam, A. R., & Raftari, M. (2014b). Characteristics of continuous unidirectional kenaf fiber reinforced epoxy composites. *Materials and Design*, 64(September), 640–649. <https://doi.org/10.1016/j.matdes.2014.08.010>
- Maulana, M. R., Sugiman, S., Ahmad, H., & Jaini, Z. M. (2022). *Strength Predictions of Notched Foam Concrete Beam Strengthened With KFRP Plates Under Flexural Load* (under review - Construction and Building Materials)
- Misnon, M. I., Islam, M. M., Epaarachchi, J. A., & Lau, K. tak. (2014). Potentiality of utilizing natural textile materials for engineering composites applications. *Materials and Design*, 59, 359–368. <https://doi.org/10.1016/j.matdes.2014.03.022>
- Nambiar, E. K. K., & Ramamurthy, K. (2006). Influence of filler type on the properties of foam concrete. *Cement and Concrete Composites*, 28(5), 475–480. <https://doi.org/10.1016/j.cemconcomp.2005.12.001>
- NCHRP-549. (2005). Simplified Shear Design of Structural Concrete Members: Appendixes. In *Simplified Shear Design of Structural Concrete Members: Appendixes*. <https://doi.org/10.17226/22070>
- Omar, Z., S.Sugiman, M.M. Yusoff, H. Ahmad (2022). Material and Independent properties of Kenaf FRP Composites. Proceeding in the 1st MIMSE 2022, University of Mataram, Indonesia.
- Oren, O. H., Gholampour, A., Gencel, O., & Ozbakkaloglu, T. (2020). Physical and mechanical properties of foam concretes containing granulated blast furnace slag as fine aggregate. *Construction and Building Materials*, 238, 117774. <https://doi.org/10.1016/j.conbuildmat.2019.117774>
- Sang, G., Zhu, Y., Yang, G., & Zhang, H. (2015). Preparation and characterization of high porosity cement-based foam material. *Construction and Building Materials*, 91, 133–137. <https://doi.org/10.1016/j.conbuildmat.2015.05.032>
- She, W., Du, Y., Zhao, G., Feng, P., Zhang, Y., & Cao, X. (2018). Influence of coarse fly ash on the performance of foam concrete and its application in high-speed railway roadbeds. *Construction and Building Materials*, 170, 153–166. <https://doi.org/10.1016/j.conbuildmat.2018.02.207>
- Sun, C., Zhu, Y., Guo, J., Zhang, Y., & Sun, G. (2018). Effects of foaming agent type on the workability, drying shrinkage, frost resistance and pore distribution of foamed concrete. *Construction and Building Materials*, 186, 833–839. <https://doi.org/10.1016/j.conbuildmat.2018.08.019>
- Yu, Z., Zhang, J., Shen, J., & Chen, H. (2021). Simulation of crack propagation behavior of nuclear graphite by using XFEM, VCCT and CZM methods. *Nuclear Materials and Energy*, 29, 101063. <https://doi.org/10.1016/j.nme.2021.101063>